DOI: 10.1002/ejic.200900067

Bis(terdentate) Pyrazole/Pyridine Ligands: Synthesis, Crystal Structures and Magnetic Properties of Bridged Binuclear and Tetranuclear Copper(II) Complexes

Akhilesh Kumar Singh,[a] Jarl Ivar van der Vlugt,[a][‡] Serhiy Demeshko,[a] Sebastian Dechert,[a] and Franc Meyer*[a]

Keywords: N ligands / Copper / Dinuclear complexes / Magnetic properties

A new binucleating bis(terdentate) ligand, 3,5-[3-bis(2-pyridyl)pyrazole-1-ylmethyl]pyrazole (HL^2), was synthesized. Reaction of the deprotonated ligand L^2 with hydrated Cu^{II} salts gives (μ-pyrazolato)(μ-hydroxido)-bridged binuclear and tetranuclear complexes $[L^2Cu_2(\mu\text{-}OH)(ClO_4)(MeCN)](ClO_4)$ (**2**), $[L^2Cu_2(dmf)_2(\mu_3\text{-}OH)]_2(ClO_4)_4\cdot 4dmf$ (**3**·4dmf) and $[L^2L'Cu_2](ClO_4)_2$ [**4**; HL′ = 3-(2-pyridyl)pyrazole]. In these complexes, both μ-OH and μ_3-OH bridges were observed. This contrasts the situation for a dicopper(II) complex of the related bis(terdentate) ligand 3,5-bis[6(2,2′-dipyridyl)]pyrazole (HL^1), $\{L^1Cu_2(OMe)(MeOH)[\kappa^1\text{-}O\text{-}(NO_3)]\}\{[Cu_2(NO_3)_2(\mu\text{-}OMe)_2]\}_{0.5}\cdot MeOH$ (**1**·MeOH), where the shorter and more rigid ligand side arms enforce a larger Cu···Cu separation and the formation of a MeO–HOMe moiety within the bimetallic pocket. Molecular structures of all complexes were elucidated by X-ray crystallography. Variable-temperature magnetic susceptibility measurements (295–2 K) for powdered samples of complexes **2**–**4** reveal strong antiferromagnetic coupling between two copper centres. The magnitude of the coupling is discussed in view of the structural features. During the preparation of complex **4**, partial ligand hydrolysis was also observed, but this strongly depends on the reaction conditions.

Introduction

Among the N-heterocycles, pyrazoles and pyridines are probably the most prominent systems used in coordination chemistry. Deprotonated pyrazoles have a high tendency to span two metal ions as *N*,*N*′-bridging ligands.[1] Introduction of chelating side arms at the 3- and 5-positions of the central pyrazolate then allows control of crucial parameters, such as the metal–metal separation (by the lengths of the side arms)[2] or the coordinative saturation and electronic properties of the bimetallic array (by the number and type of side arm donor atoms).[3] If suitably oriented binding sites at the metal ions are accessible, the dinuclear entities may serve as building blocks for the targeted assembly of oligonuclear or extended coordination compounds.[4] On the other side, a plethora of chelating pyridine-based ligands are known, and the bipyridine and terpyridine families are probably the most abundant.[5,6] We recently reported a new hybrid ligand system HL^1 that combines favourable characteristics of the two different ligand classes.[7] The central pyrazole may serve as a bridging unit, and together with the appended bipyridyl arms provides two terdentate (terpyridine-like) binding pockets in a rigid and highly preorganized arrangement.

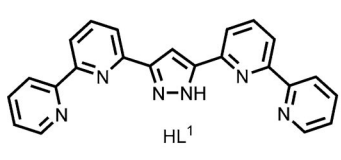

HL^1

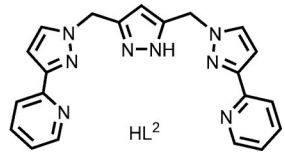

HL^2

Once deprotonated, the HL^1 ligand was shown to preferably give compact and highly stable [2 × 2] grid complexes with a variety of 3d transition-metal ions such as Mn^{2+}, Fe^{2+}, Co^{2+} and Cu^{2+}.[7,8] Whereas distorted octahedral $\{N_6\}$-environments composed of two terdentate compartments from two perpendicular $[L^1]^-$ ligand strands were found for Mn^{2+}, Fe^{2+} and Co^{2+}, the Jahn–Teller ion Cu^{2+} featured only five coordination with one peripheral pyridyl group of each ligand strand dangling. This suggested that coordination motives other than the [2 × 2] grid-type could possibly be achieved with ligand HL^1 and Cu^{2+} under appropriate conditions, which is now confirmed in this paper.

In addition, in the present work we introduce a new binucleating pyrazole/pyridine hybrid ligand HL^2 that bears pyridylpyrazole (pypz) side arms. Pyridylpyrazole has pre-

[a] Institut für Anorganische Chemie, Georg-August-Universität Göttingen,
Tammannstrasse 4, 37077 Göttingen, Germany
E-mail: franc.meyer@chemie.uni-goettingen.de
[‡] Current address: Supramolecular & Homogeneous Catalysis Group, van't Hoff Institute for Molecular Sciences, University of Amsterdam,
Nieuwe Achtergracht 166, 1018 WV Amsterdam, The Netherlands

Supporting information for this article is available on the WWW under http://dx.doi.org/10.1002/ejic.200900067.

viously been attached to a variety of spacers, giving valuable chelating ligand scaffolds.[9] Formally, HL^2 differs from HL^1 by the replacement of the hinge pyridines in HL^1 by pyrazole units, which gives rise to different chelate ring sizes when metal ions are hosted in both binding compartments for the two ligands: 5/5 in HL^1 vs. 6/5 in HL^2. Whereas both ligands feature two adjacent terdentate $\{N_3\}$ binding pockets, their mutual disposition should prevent the formation of grid complexes with perpendicular ligand strands in the case of HL^2. A series of (μ-pyrazolato)(μ-hydroxido)-bridged copper(II) complexes of the new ligand HL^2 as well as a (μ-pyrazolato)(μ-MeOH···OMe)-bridged copper(II) complex of HL^1 are presented here, together with their spectral and magnetic properties.

Results and Discussion

Synthesis and General Characterization

The new bis(terdentate) ligand HL^2 (Scheme 1) was synthesized by treating THP-protected 3,5-bis(chloromethyl)-pyrazole[10] with 3-(2-pyridyl)pyrazole (pypz, 2 equiv.)[11] (deprotonated with NaH) in THF and subsequent acidic removal of the protecting group. HL^2 was isolated as a white shiny solid and characterized by NMR and IR spectroscopy as well as by elemental analysis.

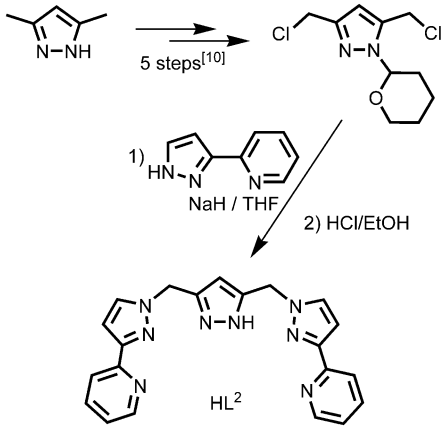

Scheme 1. Synthetic route for the new bis(terdentate) pyrazolate-based compartmental ligand HL^2.

In order to probe the coordination properties of the new HL^2 ligand in comparison to those of the more rigid and constrained HL^1 ligand, copper(II) complexes of both ligands were prepared. Deprotonation of the HL^1 ligand with NaO*t*Bu in MeOH followed by the addition of $Cu(NO_3)_2{\cdot}3H_2O$ (2 equiv.) gave a blue-green reaction mixture. Subsequent slow diffusion of diethyl ether into the concentrated MeOH solution led to the formation of blue single crystals, suitable for X-ray crystallography, of compound **1**·MeOH, $[L^1Cu_2(OMe)(MeOH)(\kappa^1\text{-}O\text{-}(NO_3))]\{(Cu_2(NO_3)_2(\mu\text{-}OMe)_2)\}_{0.5}{\cdot}$MeOH.

The blue complex $[L^2Cu_2(\mu\text{-}OH)(ClO_4)(MeCN)](ClO_4)$ (**2**) was produced when the ligand HL^2 was first deprotonated by NaO*t*Bu or KO*t*Bu in MeOH solution and subsequently treated with $[Cu(H_2O)_6](ClO_4)_2$ (2 equiv.). Alternatively, $[Mn(OAc)_2]{\cdot}4H_2O$ can be used as a base without formation of heterobimetallic complexes, even if equimolar amounts of the two different metal salts are used. When deprotonation of HL^2 was carried out by using NaO*t*Bu in water and $[Cu(H_2O)_6](ClO_4)_2$ was added, a blue precipitate formed. Dissolution of this crude precipitate in dmf and slow diffusion of ethyl acetate into the solution produced blue single crystals of the tetranuclear complex $[L^2Cu_2(\mu_3\text{-}OH)(dmf)_2]_2(ClO_4)_4{\cdot}4$dmf (**3**·4dmf). In a further variation of the reaction conditions, $[Mn(OAc)_2]{\cdot}4H_2O$ was used as a base in a water/MeOH mixture (1:1) and $[Cu(H_2O)_6](ClO_4)_2$ was added subsequently. Interestingly, partial ligand hydrolysis was reproducibly observed under these conditions to give some free side arm 3-(2-pyridyl)pyrazole (pypz) that coordinates as an additional bridge between the two copper ions in the resulting product $[L^2Cu_2(pypz)](ClO_4)_2$ (**4**). Similar hydrolytic cleavage reactions have previously been observed for other ligands containing the pypz moiety.[12] Careful screening of reaction conditions and products revealed that hydrolysis of HL^2 in the presence of Cu^{2+} takes place only when water is in excess in the reaction medium, whereas the use of hydrated metal salts in pure MeOH does not cause any significant ligand degradation. In the case of pure water as the solvent, rapid precipitation of the insoluble copper(II) complex apparently prevents ligand hydrolysis.

Molecular structures of complexes **1**–**4** were determined by X-ray crystallography and are shown in Figures 1–4. Table 1 includes selected distances and the parameter τ that characterizes the coordination geometry in the continuum between square pyramidal ($\tau = 0$) and trigonal bipyramidal ($\tau = 1$).[13] For both dinuclear complexes **1** and **2** the copper atoms are found in a distorted square pyramidal environment (Figures 1 and 2). The basal plane consists of three nitrogen atoms from the binucleating ligand and one oxygen atom from a bridging OH (**2**) or MeOH···OMe group (**1**). The major difference in the molecular cores is the Cu···Cu separation that strongly depends on the length of the chelating side arms and the size of the chelate rings formed between the ligand and the metal ions. Five-membered chelate rings of the type N–C_2–N–Cu in **1** pull the metal ions back and apart and enforce a much larger Cu···Cu separation (≈4.38 Å) in comparison to **2** containing six-membered chelate rings of the type N–C_2–N–N–Cu (≈3.29 Å). Whereas in the latter case, an OH bridge can be accommodated in the bimetallic pocket, the Cu···Cu distance in **1** prevents a bridging position of small ions (such as HO^- or MeO^-), but requires incorporation of an additional solvent molecule to give, for example, the MeOH···OMe unit observed here. Similar effects of the side arm topology have been described previously for other pyrazolate-based systems.[14] Apical positions of the copper ions in **1** and **2** are occupied by either oxygen atoms from nitrate (**1**) or perchlorate (**2**) or nitrogen atoms from coordinating acetonitrile solvent molecules (**2**). As expected for the Jahn–Teller ion Cu^{2+}, distances to the apical donor atoms are much longer than those within the basal plane.

Nitrate anions and the dinuclear cations in **1** form a polymeric chain in the solid state, where the bimetallic building blocks are linked through O,O′-bridging nitrate. The remaining charge of the chain is compensated by the complex anion $[\{(NO_3)_2Cu\}_2(\mu\text{-}OMe)_2]^{2-}$. A more detailed description of this unique anion, which represents the first structurally characterized example of a μ-OMe bridged dicopper tetranitrate dianion, is given in the Supporting Information.

Table 1. Interatomic distances [Å] and τ-values for **1**–**4**.

	1·MeOH	**2**	**3**·4dmf	**4**
Cu–N (basal)	1.95–2.08	1.94–2.03	1.95–2.08	1.92–2.17
Cu–N (apical)	–	2.28	–	2.28
Cu–O (basal)	1.89/1.90	1.91/1.94	1.94/1.96	–
Cu–O (apical)	2.37/2.32	2.61	2.22–2.60	2.56/2.58
Cu1···Cu2	4.38	3.29	3.34	3.55
τ (Cu1)	0.36	0.15	0.02	–
τ (Cu2)	0.22	0.08	–	0.45

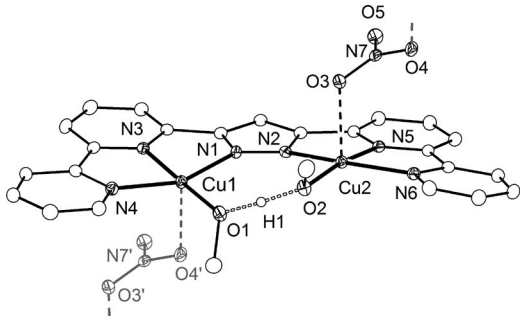

Figure 1. ORTEP plot (30% probability thermal ellipsoids) of the molecular structure of **1**·MeOH. For the sake of clarity most of the hydrogen atoms, the solvent molecules and the $[\{(NO_3)_2Cu\}_2(\mu\text{-}OMe)_2]^{2-}$anion are omitted. Selected distances [Å] and angles [°]: Cu1–O1 1.8936(16), Cu1–N3 1.9460(19), Cu1–N1 2.0099(19), Cu1–N4 2.042(2), Cu1–O4 2.3658(18), Cu2–O2 1.9008(16), Cu2–N5 1.962(2), Cu2–N2 2.031(2), Cu2–N6 2.077(2), Cu2–O3 2.3238(18), Cu1···Cu2 4.3809(5), Cu1···Cu2′ 5.9303(5), O1···O2 2.420(2); O1–Cu1–N3 178.51(8), O1–Cu1–N1 99.18(8), N3–Cu1–N1 79.68(8), O1–Cu1–N4 101.44(8), N3–Cu1–N4 79.51(8), N1–Cu1–N4 156.90(8), O1–Cu1–O(4)′ 91.64(7), N3–Cu1–O4′ 89.36(7), N1–Cu1–O4′ 92.19(7), N4–Cu1–O4′ 97.49(7), O2–Cu2–N5 170.28(8), O2–Cu2–N2 98.58(8), N5–Cu2–N2 79.14(8), O2–Cu2–N6 102.30(7), N5–Cu2–N6 78.67(8), N2–Cu2–N6 157.02(8), O2–Cu2–O3 93.82(7), N5–Cu2–O3 95.78(7), N2–Cu2–O3 94.56(7), N6–Cu2–O3 93.52(7), O1–H1···O2 177(4). Symmetry transformation used to generate equivalent atoms (′): –1 + *x*, *y*, *z*.

Related compound **3**, which was obtained from dmf/ethyl acetate, is composed of bimetallic building blocks $[L^2Cu_2(OH)]^{2+}$ that are similar to **2**, but with dmf solvent molecules in apical positions (Figure 3). In this case, however, two of these entities are symmetry related and are linked by additional interactions between the OH group from one subunit with the Cu2 atom of the second subunit, giving rise to a strongly Jahn–Teller distorted octahedral situation for the two central metal ions [*d*(Cu2–O1′) = 2.5377(15) Å] in an overall tetranuclear array. A rather short Cu···Cu distance results for the central $Cu_2(\mu\text{-}OH)_2$ rhomb in **3** (3.25 Å). Elongated octahedral coordination is also observed for one of the two copper atoms in **4**, in this case with two oxygen atoms from perchlorate anions occu-

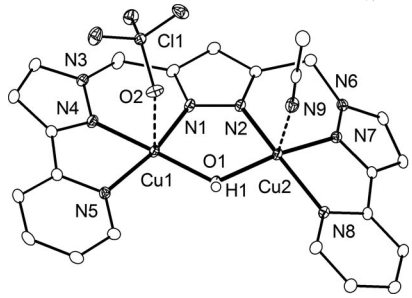

Figure 2. ORTEP plot (30% probability thermal ellipsoids) of the molecular structure of **2**. For the sake of clarity most of the hydrogen atoms and one ClO_4^- anion are omitted. Selected distances [Å] and angles [°]: Cu1–O1 1.9072(19), Cu1–N4 1.940(2), Cu1–N1 1.942(2), Cu1–N5 2.017(2), Cu1–O2 2.615(2), Cu2–O1 1.9367(19), Cu2–N2 1.956(2), Cu2–N7 1.974(2), Cu2–N8 2.032(2), Cu2–N9 2.278(2), Cu1···Cu2 3.2854(5); O1–Cu1–N4 177.18(9), O1–Cu1–N1 91.86(9), N4–Cu1–N1 87.38(10), O1–Cu1–N5 99.96(9), N4–Cu1–N5 80.71(10), N1–Cu1–N5 168.02(9), O1–Cu1–O2 92.16(8), N4–Cu1–O2 90.62(8), N1–Cu1–O2 95.56(8), N5–Cu1–O2 85.94(8), O1–Cu2–N2 91.03(9), O1–Cu2–N7 164.43(9), N2–Cu2–N7 86.50(9), O1–Cu2–N8 98.51(8), N2–Cu2–N8 159.54(9), N7–Cu2–N8 79.44(9), O1–Cu2–N9 95.33(9), N2–Cu2–N9 98.33(9), N7–Cu2–N9 100.24(9), N8–Cu2–N9 98.74(9), Cu1–O1–Cu2 117.45(10).

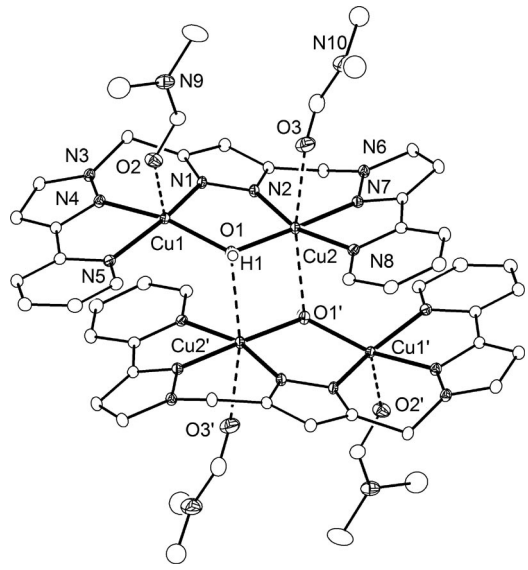

Figure 3. ORTEP plot (30% probability thermal ellipsoids) of the molecular structure of **3**·4dmf. For the sake of clarity most of the hydrogen atoms, disorder, solvent molecules and ClO_4^- anions are omitted. Selected distances [Å] and angles [°]: Cu1–O1 1.9555(14), Cu1–N1 1.9637(17), Cu1–N4 1.9767(17), Cu1–N5 2.0755(17), Cu1–O2 2.2205(16), Cu2–O1 1.9372(15), Cu2–N2 1.9536(17), Cu2–N7 1.9555(17), Cu2–N8 2.0609(17), Cu2–O1′ 2.5377(15), Cu2–O3 2.6031(19), Cu1···Cu2 3.3372(4), Cu2···Cu2′ 3.2449(5), Cu1···Cu2′ 3.7292(4), O1–Cu1–N1 89.59(7), O1–Cu1–N4 161.30(7), N1–Cu1–N4 86.08(7), O1–Cu1–N5 102.25(6), N1–Cu1–N5 162.30(7), N4–Cu1–N5 78.50(7), O1–Cu1–O2 102.21(7), N1–Cu1–O2 107.71(7), N4–Cu1–O2 96.44(7), N5–Cu1–O2 82.84(6), O1–Cu2–N2 89.51(7), O1–Cu2–N7 176.06(7), N2–Cu2–N7 86.68(7), O1–Cu2–N8 104.61(7), N2–Cu2–N8 163.67(7), N7–Cu2–N8 79.31(7), O1–Cu2–O1′ 88.04(6), N2–Cu2–O1′ 100.83(6), N7–Cu2–O1′ 91.68(6), N8–Cu2–O1′ 88.03(6), O1–Cu2–O3 96.05(7), N2–Cu2–O3 93.37(7), N7–Cu2–O3 85.19(7), N8–Cu2–O3 77.25(6), O1′–Cu2–O3 165.27(6), Cu1–O1–Cu2 118.03(8). Symmetry transformation used to generate equivalent atoms (′): –*x*, –*y*, 1 – *z*.

pying the axial positions at long distances [Figure 4; *d*(Cu1–O5) = 2.5586(13) Å, *d*(Cu1–O1) = 2.5832(14) Å]. The second copper atom in **4** is surrounded by five nitrogen atoms from the binucleating ligand scaffold and the pypz coligand (which results from ligand hydrolysis, see above), with a geometry intermediate between square pyramidal and trigonal bipyramidal (τ = 0.45). Similar to the situation in **2**, the Cu···Cu distance in **3** and **4** is relatively short (3.34 and 3.55 Å, respectively), but the ligand scaffold $[L^2]^-$ apparently is flexible enough to allow adaptation of the Cu···Cu separation to coligands of different size requirements, such as the OH group in **3** or the second pyrazolate bridge in **4**.

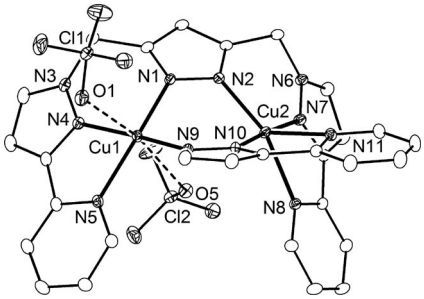

Figure 4. ORTEP plot (30% probability thermal ellipsoids) of the molecular structure of **4**. For the sake of clarity hydrogen atoms are omitted. Selected distances [Å] and angles [°]: Cu1–N9 1.9395(15), Cu1–N4 1.9417(15), Cu1–N1 1.9875(15), Cu1–N5 2.0835(15), Cu1–O5 2.5586(13), Cu1–O1 2.5832(14), Cu2–N10 1.9209(15), Cu2–N7 1.9311(15), Cu2–N2 1.9868(14), Cu2–N8 2.1710(14), Cu2–N11 2.2811(15), Cu1···Cu2 3.5466(3), N9–Cu1–N4 169.79(6), N9–Cu1–N1 97.90(6), N4–Cu1–N1 89.11(6), N9–Cu1–N5 96.91(6), N4–Cu1–N5 78.16(6), N1–Cu1–N5 160.01(6), N9–Cu1–O5 87.29(5), N4–Cu1–O5 100.60(5), N1–Cu1–O5 86.50(5), N5–Cu1–O5 80.86(5), N9–Cu1–O1 90.40(5), N4–Cu1–O1 80.56(6), N1–Cu1–O1 105.26(5), N5–Cu1–O1 87.96(5), O5–Cu1–O1 168.22(5), N10–Cu2–N7 175.15(6), N10–Cu2–N2 95.88(6), N7–Cu2–N2 88.78(6), N10–Cu2–N8 99.47(6), N7–Cu2–N8 77.08(6), N2–Cu2–N8 147.89(6), N10–Cu2–N11 76.72(6), N7–Cu2–N11 99.21(6), N2–Cu2–N11 131.01(6), N8–Cu2–N11 80.21(5).

Intra- or intermolecular hydrogen bonding of the OH group is observed in **1**, **2** and **3**. Bonding parameters for **1** are listed in the legend to Figure 1. For **2** the hydrogen atom of the OH is connected to an oxygen atom from a perchlorate anion [*d*(O···O) = 3.101(3) Å; angle O–H···O 172(4)], and in **3** the oxygen atom of a dmf is the hydrogen-bond acceptor [*d*(O···O) = 2.813(2) Å; angle O–H···O 178(3)]. A closer inspection of the crystal packing diagrams of **2** and **3** reveals that these molecules are engaged in π···π stacking interactions in the solid state. A more detailed description of these interactions and corresponding Figures are given in the Supporting Information.

Solution absorption spectra for all complexes are displayed in Figure 5. Copper(II) complexes usually feature ligand field transitions in the range 630–1100 nm. A broad absorption at around 670 (**1**) or 640 nm (**2**–**4**) is observed for the present set of complexes, which is characteristic for square pyramidal copper(II). Spectra for **2** and **4** exhibit a pronounced shoulder around 820–830 nm. Given the similarity of the spectrum for **3** (broad absorption band at 634 nm) and those of the other complexes, one might suspect that the tetranuclear array observed in the solid state breaks down to bimetallic species in solutions of coordinating solvents such as dmf. The UV region of the electronic

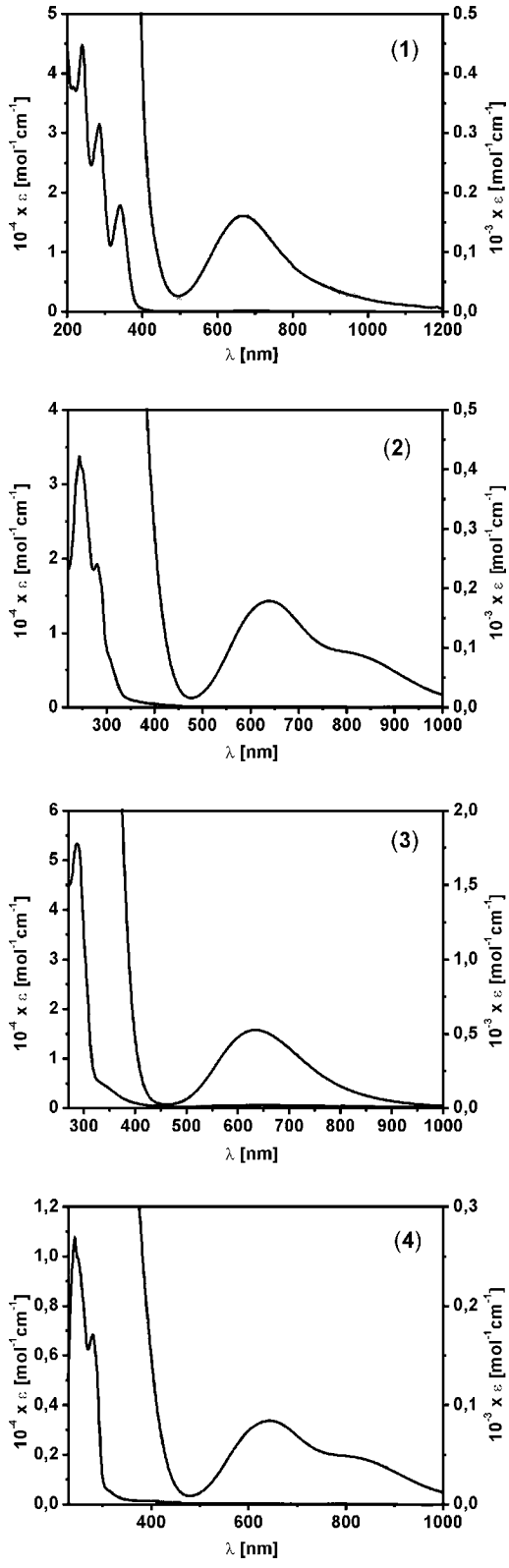

Figure 5. UV/Vis spectra of complexes **1** (in MeOH), **2** (in MeCN), **3** (in dmf) and **4** (in MeCN) (from top).

spectra is characterized by the usual intraligand π–π* (and possibly LMCT) bands around 285 and 240 nm, though with a distinctly different pattern for complexes of $[L^1]^-$ versus $[L^2]^-$. Additional absorptions appear at 341 (**1**), 315 (**2**) or 320 nm (**4**), that is, at lowest energy in the case of the most extended planar ligand system $[L^1]^-$ featuring directly linked aromatic rings.

In the IR spectrum of complex **2**, a strong split band around 1088 cm^{-1} and a medium intensity band at 624 nm result from coordinated ClO_4^-. For complex **3**·4dmf, the bands corresponding to ClO_4^- are observed at 1092 and 623 cm^{-1}.

Continuous wave EPR spectra (X-band) of powdered samples of **2**–**4** show broad signals centred around 3000 G ($g \approx 2.12$). Signals are weakest in the case of **3**, in accordance with the strongest antiferromagnetic coupling in that system (see below). In the case of **2** and **4** weak half-field signals are discernible, characteristic of exchange-coupled dicopper(II) systems with an $S = 0$ ground state.

Magnetic Properties

Magnetic susceptibility measurements were carried out on complexes **2**–**4** at a magnetic field of 5000 Oe in the temperature range 295–2.0 K. The temperature dependence of the magnetic susceptibility χ_M and of the product $\chi_M T$ are shown in Figure 6. Experimental data for complexes **2**, **3**·4dmf and **4** were modelled by using a fitting procedure to the appropriate Heisenberg–Dirac–van-Vleck (HDvV) spin Hamiltonian for isotropic exchange coupling and Zeeman splitting [Equation (1)].[15]

$$\hat{H} = -2J\hat{S}_1\hat{S}_2 + g\mu_B(\hat{S}_1+\hat{S}_2)B \quad (1)$$

Temperature-independent paramagnetism (TIP) and a Curie-behaved paramagnetic impurity (PI) with spin $S = 1/2$ were included according to $\chi_{calcd.} = (1 - PI)\chi + PI\chi_{mono} + TIP$.[16] For all complexes **2**, **3** and **4**, the product $\chi_M T$ at 295 K is considerably lower than the theoretical value expected for two or more uncoupled copper(II) ions. $X_M T$ further decreases when the temperature is lowered to 2 K, which is indicative of dominant antiferromagnetic interactions. Least-squares fitting gave the set of magnetic parameters $J = -110$ cm^{-1} (for **2**), -153 cm^{-1} (for **3**·4dmf) and -102 cm^{-1} (for **4**; Table 2). Given that the interaction between the binuclear subunits in **3** is only weak [the Cu2–O1′ bond is very long (2.5377(15) Å) and perpendicular to the magnetic $d_{x^2-y^2}$ orbitals of the copper(II) ions] it is reasonable to assume that the magnetic properties are determined by the coupling within the subunits. Indeed, the magnetic data of **3** are well simulated by the simple dimer model.

The significant antiferromagnetic coupling observed for all complexes is due to the large σ in-plane overlap between the coplanar $d_{x^2-y^2}$ magnetic orbitals and the bridging units. It is known that the magnitude and nature of the interaction in Cu(μ-OH)$_2$Cu complexes depends on several structural parameters such as the Cu–O–Cu angle α (for $\alpha >$ 97.5° coupling is antiferromagnetic and becomes stronger as the α value increases),[17] Cu–O distances[18] and out-of-plane displacement of the hydrogen atom in the hydroxido group.[19] Cu–O–Cu angles in **2** and **3**·4dmf are relatively

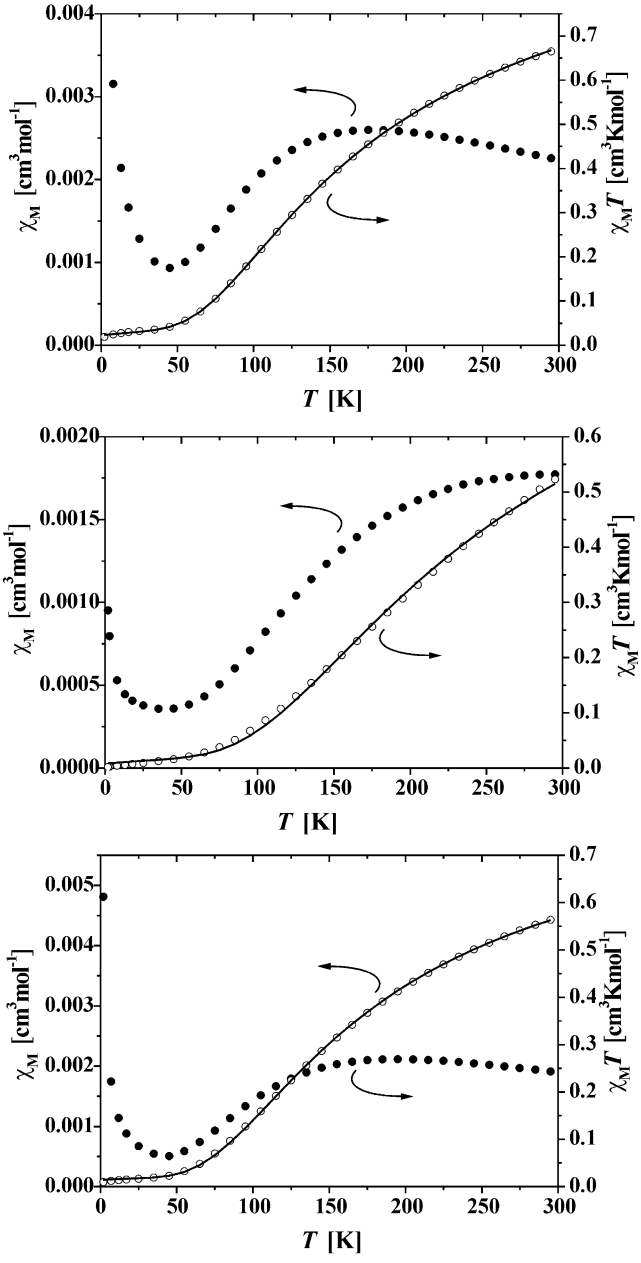

Figure 6. Plots of χ_M and $\chi_M T$ vs. T for **2**, **3**·4dmf and **4**; the solid lines represent the simulated curves.

Table 2. Parameters obtained from simulation of the SQUID data.

	g	J [cm^{-1}]	PI [%]	TIP/10^{-4} [$cm^3\,mol^{-1}$]
2	2.05	–110	3.8	1.3
3·4dmf	2.13	–153	2.1	2.0 (fixed)
4	2.11	–102	6.0	3.2

wide (≈118°) and clearly fall in the antiferromagnetic regime.

Several structural parameters also determine the magnetic coupling in Cu(μ-pyrazolato)$_2$Cu complexes. Known dicopper(II) complexes that are spanned by two pyrazolate bridges often feature square-planar or tetragonal surroundings of the metal ions, and the $d_{x^2-y^2}$ orbitals are located within the plane of the bridging heterocycles.[20–22] Previous magnetostructural considerations have identified various parameters that determine the strength of the antiferromagnetic coupling: (i) the distortion of copper(II) coordination geometry from square pyramidal towards trigonal bipyramidal,[22] (ii) the deviation from coplanarity of the pyrazolate planes and of the copper coordination planes,[23] (iii) the Cu–N–N angle [taking the difference δ(CuNN) between the deviations of the Cu–N–N and Cu–N′–N′ angle with respect to an optimum angle as a structural parameter][24] and (iv) the bending angles $\delta_{pz-bend}$.[22] Those parameters essentially reflect the asymmetry or distortion of the Cu(μ-pyrazolato)$_2$Cu central core, which effects the overlap between the magnetic copper atomic orbitals and the pyrazolate ligand orbitals. For bis(μ-pyrazolato)-bridged dicopper(II) compounds J has usually been found in the range –70 to –160 cm^{-1}.[20,22,25] There are only few examples with antiferromagnetic coupling stronger than –200 cm^{-1},[21] with the maximum value –243 cm^{-1}.[21c] The geometry of the five-coordinate Cu2 ion in **4** is distorted from SP-5 towards TBP-5 [τ(Cu2) = 0.45], and the Cu(μ-pyrazolato)$_2$Cu central core is not planar with $\delta_{pz-bend}$ = 5.5/22.0° and δ_{pz-pz} = 34.1°. In view of these structural parameters the coupling constant should be relatively moderate, and hence J = –102 cm^{-1} for **4** is in accordance with expectations.

The multitude of parameters involved for the two individual bridging units complicates the establishing of magnetostructural correlations for (μ-hydroxido)(μ-pyrazolato)-bridged dicopper(II) complexes such as **2** and **3**, because the coupling depends on the geometry of individual μ-hydroxido and μ-pyrazolato fragments and can also have diverse influences from the interplay of the bridges.[26] The combination of hydroxido and pyrazolato bridges usually is an orbital complementarity case that leads to stronger antiferromagnetic coupling. For the limited number of known complexes with this structural motif, coupling parameters have been found in the broad range –82 to –385 cm^{-1}.[26,27] Escrivà et al.[27a] proposed a rough correlation between the J values and the dihedral angle between basal coordination planes of the copper ions: the coupling should be stronger if the deviation from planarity (i.e., deviation from 0 or 180°) increases. This parameter is 9.9° for **2** and 8.7° for **3**. Both values are similar and J parameters (Table 2) have the same order of magnitude. The somewhat stronger coupling in **3** may be explained by the slightly larger Cu–O–Cu angle (117.5° in **2** vs. 118.0° in **3**) as well as by better overlap between the coplanar $d_{x^2-y^2}$ magnetic orbitals and the bridging pyrazolate as a result of the smaller $\delta_{pz-bend}$ (representing the dihedral angle of the pyrazolate plane relative to the Cu–N–N–Cu plane, 5.8° in **2** vs. 2.7° in **3**).

Conclusions

The new ligand HL^2 complements the variety of available binucleating pyrazolate ligands and represents a close analogue of HL^1. Both ligands feature two terdentate {N$_3$} compartments, but with different chelate ring sizes and greater flexibility in the case of HL^2, which has drastic consequences for the resulting metal···metal separations. HL^2 proved very suited to host two copper(II) ions, but may be susceptible to metal-mediated ligand hydrolysis depending on the reactions conditions. The structural and magnetic characterization of **2**, **3** and **4** provides further examples of the still limited number of dicopper(II) complexes with Cu(μ-pyrazolato)$_2$Cu and mixed-bridged Cu(μ-pyrazolato)(μ-OH)Cu cores. Typical ranges of coupling constants J and relevant structural parameters for these motifs have been re-evaluated, and values for the present new complexes add to the body of data that will eventually lead to a more comprehensive magnetostructural correlation for these popular bridging units.

Experimental Section

Caution! Although no problems were encountered in this work, transition-metal perchlorates are potentially explosive and should be handled with care and proper precautions.

General: All chemicals were purchased from commercial sources and used as received. HL^1,[7] pyridylpyrazole[11] and THP-protected 3,5-bis(chloromethyl)pyrazole[10] were prepared by following literature methods. Microanalyses were performed by the Analytical Laboratory in the institute of Inorganic Chemistry at Georg-August-University Göttingen. IR spectra were recorded as KBr pellets by using a Digilab Excalibur, and UV/Vis spectra were measured with a Varian Cary 5000 spectrometer. Mass spectra (EI) were recorded with a Finnigan MAT 95 spectrometer. Continuous wave (CW) EPR spectra were measured with a Bruker ELEXSYS E500 spectrometer, equipped with a digital temperature control system ER 4131VT. All spectra were recorded on powdered samples at 290 K, at about 9.44 GHz microwave frequency, 8 G field modulation amplitude, 100 kHz field modulation frequency, and around 12.6 mW microwave power. Susceptibility measurements were carried out with a Quantum-Design MPMS-5S SQUID magnetometer equipped with a 5 T magnet in the range from 290 to 2.0 K. The powdered samples were contained in a gel bucket and fixed in a nonmagnetic sample holder. Each raw data file for the measured magnetic moment was corrected for the diamagnetic contribution of the sample holder and the gel bucket. The molar susceptibilities were corrected by using Pascal's constants and the increment method.

3,5-Bis[3-(2-pyridyl)pyrazole-1-ylmethyl]pyrazole (HL^2): To a solution of 3-(2-pyridyl)pyrazole (1.312 g, 9.05 mmol) in THF (40 mL) under an atmosphere of dry nitrogen was added solid NaH (0.258 g, 10.78 mmol) portionwise. The reaction mixture was stirred for 30 min, during which time the solution turned light yellow. A solution of 3,5-bis(chloromethyl)-1-(tetrahydropyran-2-yl)-1*H*-pyrazole (1.0 g, 4.31 mmol) in THF (10 mL) was added slowly dropwise with continuous stirring. Stirring was continued for 24 h at room temperature. After that, the solvent was removed completely, and the residue was dissolved in water and filtered to dispose of the formed NaCl. The residue was dissolved in EtOH

(50 mL) and HCl (5 mL) was added to it, and the reaction mixture was heated at reflux for 3 h. A saturated solution of $NaHCO_3$ was then added with continued stirring until complete neutralization. Extraction with $CHCl_3$ and removal of the solvent yielded the crude ligand, HL^2, which was recrystallized from MeOH to yield an off-white solid ligand (1.10 g, 65%). M.p. 148 °C. ^{1}H NMR (500 MHz, [D$_6$]DMSO): δ = 5.34 (d, 4 H, pz-CH2), 6.17 (s, 1 H, pz-H), 6.80 (s, pz′-4H, 2 H), 7.26 (m, py-5H, 2H), 7.50–8.10 (m, py-3H,4H,6H, 6H), 8.54 (d, pz′-5H, 2H), 12.95 (br. s, 1 H, pz-NH) ppm. ^{13}C NMR (500 MHz, [D$_6$]DMSO): δ = 46.1, 49.4, 103.7, 104.1, 104.3, 119.1, 119.2, 122.3, 122.4,131.6, 136.6, 139.1, 149.1, 150.8, 151.2, 151.6, 151.8 ppm. IR (KBr): $\tilde{\nu}$ = 3075 (w), 2953 (w), 2853 (w), 2360 (w), 1595 (s), 1568 (m), 1491 (s), 1464 (s), 1389 (m), 1357 (m), 1321 (m), 1280 (m), 1227 (s), 1153 (m), 1052 (m), 993 (m), 760 (s) cm^{-1}. EI-MS: *m*/*z* (%) = 381.1 (100), [M]$^+$. $C_{21}H_{18}N_8$ (382.42): calcd. C 65.95, H 4.74, N 29.30; found C 65.42, H 4.76, N 28.87.

[L^{1}Cu$_2$(OMe)(MeOH){κ^1-*O*-(NO$_3$)}]{Cu$_2$(NO$_3$)$_2$(μ-OMe)$_2$}$_{0.5}$·MeOH (1·MeOH): HL^1 (100 mg, 266 μmol) and NaO*t*Bu (26 mg, 266 μmol) were dissolved in MeOH (50 mL) at room temperature. To this mixture was added dropwise a solution of $Cu(NO_3)_2{\cdot}3H_2O$ (128 mg, 532 μmol) in MeOH (25 mL) to give a blue-green solution and stirring was continued for 16 h. After filtration, the solution was concentrated to ≈10 mL in vacuo and layered with Et_2O (50 mL). Slow diffusion yielded bluish crystals of **1**·MeOH (49 mg, 21%). UV/Vis (7.6×10^{-4} M, MeOH): λ (ε, L mol^{-1} cm^{-1}) = 670 (160), 341 (17826), 285 (31464), 240 (44714) nm. FAB-MS (glycerine): *m*/*z* (%) = 501 (100) [Cu$_2$L]$^+$. $C_{27}H_{29}Cu_3N_9O_{13}$ (878.21): calcd. C 36.93, H 3.33, N 14.35; found C 37.28, H 3.11, N 14.06.

[L^{2}Cu$_2$(μ-OH)(ClO$_4$)(MeCN)](ClO$_4$) (2): To a solution of HL^2 (100 mg, 0.262 mmol) in MeOH (10 mL) was added $[Cu(H_2O)_6](ClO_4)_2$ (194 mg, 0.524 mmol) with stirring. To this reaction mixture was added $Mn(OAc)_2{\cdot}4H_2O$ (65 mg, 0.262 mmol), and the solution was stirred for an additional 5 min at room temperature. The mixture was then heated to 60 °C and stirred for 0.5 hour. The blue-coloured precipitate that appeared was filtered off and dried first in air and then in vacuo. X-ray quality single crystals of **2** were obtained by diffusion of ethyl ether into a solution of the complex in MeCN. Yield: 125 mg after drying, 62.5%. IR (KBr): $\tilde{\nu}$ = 3623 (m), 3570 (m), 3431 (br.), 3156 (m), 3136 (m), 2959 (m), 2939 (m), 2836 (m), 1634 (m), 1548 (m), 1492 (s), 1440 (m), 1355 (m), 1290 (m), 1228 (m), 1163 (s), 1061 (vs), 977 (s), 909 (s), 811 (w), 757 (m), 731 (m), 686 (m), 630 (w), 560 (w), 521 (m), 480 (w) cm^{-1}. UV/Vis (MeCN): λ (ε, L mol^{-1} cm^{-1}) = 820 (90), 640 (180), 280 (2400), 244 (4200) nm.

[L^2{(dmf)Cu}$_2$(μ$_3$-OH)]$_2$(ClO$_4$)$_4$·4dmf (3·4dmf): A suspension of HL^2 (250 mg, 0.654 mmol) in water (10 mL) was warmed with stirring and NaO*t*Bu (62 mg, 0.654 mmol) was added followed by heating the reaction mixture to 100 °C. $[Cu(H_2O)_6](ClO_4)_2$ (485 mg, 1.309 mmol) was added, and the reaction mixture was first stirred for 5 min at room temperature and then heated for 5 min to 100 °C. Stirring was continued for 2 h at room temperature. The blue-coloured precipitate that formed was filtered off and washed with MeOH, then dried first in air and then under reduced pressure. Thereafter the solid was redissolved in dmf followed by slow diffusion of ethyl acetate into this blue-coloured solution. After 7 d blue crystals of **3**·4dmf were obtained that were suitable for X-ray diffraction. Yield: 254 mg, 38% (with respect to ligand). IR (KBr): $\tilde{\nu}$ = 3623 (m), 3570 (m), 3431 (br.), 3156 (m), 3136 (m), 2959 (m), 2939 (m), 2836 (m), 1634 (m), 1548 (m), 1492 (s), 1440 (m), 1355 (m), 1290 (m), 1228 (m), 1163 (s), 1061 (vs), 977 (s), 909 (s), 811 (w), 757 (m), 731 (m), 686 (m), 630 (w), 560 (w), 521 (m), 480 (w) cm^{-1}. UV/Vis (dmf): λ (ε, L mol^{-1} cm^{-1}) = 634 (525), 340 sh (4600), 286 (53300) nm. As a result of the gradual but slow loss of dmf lattice solvent molecules upon drying, no correct elemental analysis could be obtained for **3**·4dmf.

[L^{2}Cu$_2$(pypz)](ClO$_4$)$_2$ (4): A suspension of HL^2 (100 mg, 0.261 mmol) in water (10 mL) was warmed with stirring and

Table 3. Crystal data and refinement details for **1**·MeOH, **2**, **3**·4dmf and **4**.

	1·MeOH	**2**	**3**·4dmf	**4**
Empirical formula	$C_{27}H_{29}Cu_3N_9O_{13}$	$C_{23}H_{21}Cl_2Cu_2N_9O_9$	$C_{66}H_{92}Cl_4Cu_4N_{24}O_{26}$	$C_{29}H_{23}Cl_2Cu_2N_{11}O_8$
Formula weight	878.21	765.47	2033.60	851.56
Crystal size [mm]	0.50 × 0.31 × 0.17	0.30 × 0.24 × 0.07	0.50 × 0.42 × 0.31	0.50 × 0.41 × 0.26
Crystal system	triclinic	triclinic	triclinic	triclinic
Space group	$P\bar{1}$ (No. 2)	$P\bar{1}$ (No. 2)	$P\bar{1}$ (No. 2)	$P\bar{1}$ (No. 2)
a [Å], *α* [°]	8.8104(6), 79.472(5)	10.1876(6), 109.955(4)	13.5054(5), 111.831(3)	10.2018(4), 72.858(3)
b [Å], *β* [°]	14.0493(9), 73.004(5)	11.8920(7), 99.733(4)	13.6927(5), 107.939(3)	12.4006(6), 79.495(4)
c [Å], *γ* [°]	14.4510(9), 71.932(5)	13.7674(8), 110.512(5)	14.3826(5), 103.922 (3)	13.8317(6), 78.385(3)
V [Å^3]	1617.91(18)	1519.3(3)	2150.65(18)	1623.66(12)
Z	2	2	1	2
$\rho_{calcd.}$ [g cm^{-3}]	1.803	1.833	1.570	1.742
F(000)	890	772	1048	860
μ [mm^{-1}]	2.036	1.797	1.189	1.545
T_{max}/T_{min}	0.7398/0.4377	0.8223/0.6319	0.7097/0.5380	0.7081/0.4267
hkl range	–9–10	±12	±17	±12
	±16	–15–13	±17	–14–15
	±16	±17	±18	–17–14
θ range [°]	1.53–24.77	1.67–26.97	1.70–26.94	2.00–26.94
Measured refl.	24515	13337	23399	15129
Unique refl. [R_{int}]	5524 [0.0449]	5965 [0.0444]	9318 [0.0443]	6994 [0.0325]
Observed refl. [$I > 2\sigma(I)$]	4589	5081	8417	6252
Refined parameters	482	409	570	469
Restraints	3	46	9	0
Goodness-of-fit	1.000	1.052	1.045	1.039
R_1 [$I > 2\sigma(I)$]	0.0257	0.0328	0.0353	0.0265
wR_2 (all data)	0.0678	0.0854	0.0981	0.0718
Resid. el. dens. [e Å^{-3}]	0.334/–0.329	0.773/–0.676	1.043/–0.853	0.539/–0.480

$[Cu(H_2O)_6](ClO_4)_2$ (97 mg, 0.261 mmol) was added. Then, $[Mn(OAc)_2]\cdot 4H_2O$ (96.2 mg, 0.392 mmol) was added, and the reaction mixture was heated to 100 °C. To the hot reaction mixture was added MeOH (10 mL), which caused the solution to turn clear blue. The solution was kept for slow evaporation to produce X-ray quality single crystals of **4**. Yield: 100 mg, 45%. IR (KBr): $\tilde{\nu}$ = 3431 (br.), 3134 (m), 1604 (m), 1501 (w), 1446 (s), 1439 (s), 1362 (m), 1310 (w), 1244 (m), 1120 (s), 1105 (s), 969 (w), 769 (s), 621 (s) cm^{-1}. UV/Vis (MeCN): λ (ε, $1mol^{-1}cm^{-1}$) = 830 (46), 642 (80), 320 (460), 280 (6800), 244 (10700) nm. $C_{29}H_{23}Cl_2Cu_2N_{11}O_8$ (851.56): calcd. C 40.90, H 2.72, N 18.09; found C 40.30, H 2.60, N 17.74.

X-ray Crystallography: The crystal data and details of the data collections for **1**·MeOH, **2**, **3**·4dmf and **4** are given in Table 3. X-ray data were collected with a STOE IPDS II diffractometer (graphite monochromated Mo-K_α radiation, λ = 0.71073 Å) by use of ω scans at –140 °C. The structures were solved by direct methods and refined on F^2 by using all reflections with SHELX-97.[28] Most non-hydrogen atoms were refined anisotropically. Most hydrogen atoms were placed in calculated positions and assigned to an isotropic displacement parameter of 0.08 $Å^2$. The positional and isotropic thermal parameters of the oxygen bound hydrogen atoms in **1** and **3**·4dmf were refined without any restraints or constraints. A DFIX restraint (d_{O-H} = 0.82 Å) was applied for the O–H distance in **2**. A MeOH molecule in **1** is disordered about a crystallographic centre of inversion an additionally disordered about two positions and was refined with fixed occupancies of 0.5 and 0.25. A DFIX restraint (d_{C-O} = 1.41 Å) was applied to model the disorder. Three oxygen atoms of one ClO_4^- in **2** are disordered about two positions with occupancy factors of 0.516(11) and 0.484(11). SADI restraints (Cl–O and O···O distances) were used to model the disorder. Two nitrogen carbon atoms of one dmf molecule in **3**·4dmf are disordered about two positions with occupancy factors of 0.631(14) and 0.369(14). FLAT and SADI restraints (N–C and C···C distances) and EADP constraints were used to model the disorder. Face-indexed absorption corrections were performed numerically with the program X-RED.[29] CCDC-709970 (for **1**·MeOH), -709971 (for **2**), -709972 (for **3**·4dmf) and -709973 (for **4**) contain the supplementary crystallographic data for this paper. These data can be obtained free of charge from The Cambridge Crystallographic Data Centre via www.ccdc.cam.ac.uk/data_request/cif.

Supporting Information (see footnote on the first page of this article): Intermolecular interactions in the solid state; description of the complex anion $[\{(NO_3)_2Cu\}_2(\mu\text{-}OMe)_2]^{2-}$ of **1**; EPR spectra of complexes **2**, **3** and **4**.

Acknowledgments

Financial support by the Deutsche Forschungsgemeinschaft (SFB 602, project A16) and by the Alexander-von-Humboldt Foundation (Research Fellowships to J. I. v. d. V.) is gratefully acknowledged.

[1] a) s. Trofimenko, *Prog. Inorg. Chem.* **1986**, *34*, 115–210; b) R. Mukherjee, *Coord. Chem. Rev.* **2000**, *203*, 151–218; c) J. Klingele, S. Dechert, F. Meyer, *Coord. Chem. Rev.*, DOI: 10.1016/j.ccr.2009.03.026.

[2] See, for example: a) F. Meyer, S. Beyreuther, K. Heinze, L. Zsolnai, *Chem. Ber.* **1997**, *130*, 605–613; b) F. Meyer, K. Heinze, B. Nuber, L. Zsolnai, *J. Chem. Soc., Dalton Trans.* **1998**, 207–213; c) J. Ackermann, F. Meyer, E. Kaifer, H. Pritzkow, *Chem. Eur. J.* **2002**, *8*, 247–258.

[3] See, for example: a) B. Bauer-Siebenlist, F. Meyer, E. Farkas, D. Vidovic, J. A. C. Seijo, R. Herbst-Irmer, H. Pritzkow, *Inorg. Chem.* **2004**, *43*, 4189–4202; b) T. Sheng, S. Dechert, I. Hyla-Kryspin, R. F. Winter, F. Meyer, *Inorg. Chem.* **2005**, *44*, 3863–3874; c) J. Ackermann, S. Buchler, F. Meyer, *C. R. Chim.* **2007**, *10*, 421–432.

[4] a) F. Meyer, H. Pritzkow, *Inorg. Chem. Commun.* **2001**, *4*, 305–307; b) S. Demeshko, G. Leibeling, W. Maringgele, F. Meyer, C. Mennerich, H.-H. Klauss, H. Pritzkow, *Inorg. Chem.* **2005**, *44*, 519–528; c) F. Meyer, S. Demeshko, G. Leibeling, E. Kaifer, B. Kersting, H. Pritzkow, *Chem. Eur. J.* **2005**, *11*, 1518–1526; d) S. Demeshko, G. Leibeling, S. Dechert, S. Fuchs, T. Pruschke, F. Meyer, *ChemPhysChem* **2007**, *8*, 405–417; e) F.-M. Nie, S. Demeshko, S. Fuchs, S. Dechert, T. Pruschke, F. Meyer, *Dalton Trans.* **2008**, 3971–3977.

[5] a) A. P. Smith, C. L. Fraser in *Comprehensive Coordination Chemistry II* (Eds.: J. A. McCleverty, T. J. Meyer), Elsevier, Oxford, UK, **2004**, vol. 1, p. 1–23; b) R. P. Thummel in *Comprehensive Coordination Chemistry II* (Eds.: J. A. McCleverty, T. J. Meyer), Elsevier, Oxford, UK, **2004**, vol. 1, p. 41–53.

[6] a) H. Hofmeier, U. S. Schubert, *Chem. Soc. Rev.* **2004**, *33*, 373–399; b) E. C. Constable, *Chem. Soc. Rev.* **2007**, *36*, 246–253.

[7] J. I. van der Vlugt, S. Demeshko, S. Dechert, F. Meyer, *Inorg. Chem.* **2008**, *47*, 1576–1585.

[8] B. Schneider, S. Demeshko, S. Dechert, F. Meyer, in preparation.

[9] M. D. Ward, J. A. McCleverty, J. C. Jeffery, *Coord. Chem. Rev.* **2001**, *222*, 251–272.

[10] a) T. G. Schenck, J. M. Downes, C. R. C. Milne, P. B. Mackenzie, H. Boucher, J. Whelan, B. Bosnich, *Inorg. Chem.* **1985**, *24*, 2334–2337; b) J. C. Röder, F. Meyer, H. Pritzkow, *Organometallics* **2001**, *20*, 811–817.

[11] A. J. Amoroso, A. M. C. Thompson, J. C. Jeffery, P. L. Jones, J. A. McCleverty, M. D. Ward, *J. Chem. Soc., Chem. Commun.* **1994**, 2751–2752.

[12] a) J. S. Fleming, E. Psillakis, J. C. Jeffery, K. L. V. Mann, J. A. McCleverty, M. D. Ward, *Polyhedron* **1998**, *17*, 1705–1714; b) M. J. Hallam, C. A. Kilner, M. A. Halcrow, *Acta Crystallogr., Sect. C* **2002**, *58*, m445–m446.

[13] A. W. Addison, T. N. Rao, J. Reedijk, J. van Rijn, G. C. Verschoor, *J. Chem. Soc., Dalton Trans.* **1984**, 1349–1356.

[14] a) F. Meyer, P. Rutsch, *Chem. Commun.* **1998**, 1037–1038; b) B. Bauer-Siebenlist, F. Meyer, E. Farkas, D. Vidovic, S. Dechert, *Chem. Eur. J.* **2005**, *11*, 4349–4360; A. Prokofieva, A. I. Prykhod′ko, E. A. Enyedy, E. Farkas, W. Maringgele, S. Demeshko, S. Dechert, F. Meyer, *Inorg. Chem.* **2007**, *46*, 4298–4307.

[15] O. Kahn, *Molecular Magnetism*, Wiley-VCH, Weinheim, **1993**.

[16] Simulation of the experimental magnetic data with a full-matrix diagonalisation of exchange coupling and Zeeman splitting was performed with the julX program (E. Bill: Max-Planck Institute for Bioinorganic Chemistry, Mülheim/Ruhr, Germany).

[17] V. H. Crawford, H. W. Richardson, J. R. Wasson, D. J. Hodgson, W. E. Hatfield, *Inorg. Chem.* **1976**, *15*, 2107–2110.

[18] E. Ruiz, P. Alemany, S. Alvarez, J. Cano, *Inorg. Chem.* **1997**, *36*, 3683–3688.

[19] E. Ruiz, P. Alemany, S. Alvarez, J. Cano, *J. Am. Chem. Soc.* **1997**, *119*, 1297–1303.

[20] a) B. Mernari, F. Abraham, M. Lagrenee, M. Drillon, P. Legoll, *J. Chem. Soc., Dalton Trans.* **1993**, 1707–1711; b) P. King, R. Clérac, C. E. Anson, A. K. Powell, *Dalton Trans.* **2004**, 852–861; c) C. Miranda, F. Escartí, L. Lamarque, E. Garsía-España, P. Navarro, J. Latorre, F. Lloret, H. R. Jiménez, M. J. R. Yunta, *Eur. J. Inorg. Chem.* **2005**, 189–208; d) S. Tanase, I. A. Koval, E. Bouwman, R. de Gelder, J. Reedijk, *Inorg. Chem.* **2005**, *44*, 7860–7865; e) T.-L. Hu, J.-R. Li, C.-S. Liu, X.-S. Shi, J.-N. Zhou, X.-H. Bu, J. Ribas, *Inorg. Chem.* **2006**, *45*, 162–173; f) V. Mishra, F. Lloret, R. Mukherjee, *Eur. J. Inorg. Chem.* **2007**, 2161–2170; g) Q. F. Mokuolu, D. Foguet-Albiol, L. F. Jones, J. Wolowska, R. M. Kowalczyk, C. A. Kilner, G. Christou, P. C. McGowana, M. A. Halcrow, *Dalton Trans.* **2007**, 1392–1399; h) L. Penkova, S. Demeshko, M. Haukka,

V. A. Pavlenko, F. Meyer, I. O. Fritsky, *Z. Anorg. Allg. Chem.* **2008**, *634*, 2428–2436.

[21] a) B. Mernari, F. Abraham, M. Lagrenee, M. Drillon, P. Legoll, *J. Chem. Soc., Dalton Trans.* **1990**, 195–198; b) F. Meyer, A. Jacobi, L. Zsolnai, *Chem. Ber.* **1997**, *130*, 1441–1447; c) J. Teichgräber, G. Leibeling, S. Dechert, F. Meyer, *Z. Anorg. Allg. Chem.* **2005**, *631*, 2613–2618; d) D. J. de Geest, A. Noble, B. Moubaraki, K. S. Murray, D. S. Larsena, S. Brooker, *Dalton Trans.* **2007**, 465–475.

[22] H. Matsushima, H. Hamada, K. Watanabe, M. Koikawa, T. Tokii, *J. Chem. Soc., Dalton Trans.* **1999**, 971–977 and references cited therein.

[23] D. Ajò, A. Bencini, F. Mani, *Inorg. Chem.* **1988**, *27*, 2437–2444.

[24] V. P. Hanot, T. D. Robert, J. Kolnaar, J. P. Haasnoot, J. Reedijk, H. Kooijman, A. L. Spek, *J. Chem. Soc., Dalton Trans.* **1996**, 4275–4281.

[25] Reported values have been adapted for $\hat{H} = -2J\hat{S}_1\hat{S}_2$ Hamiltonian. Ranges for *J* values of bis(μ-pyrazolato)-bridged dicopper(II) compounds given in previous work[21c] are partly erroneous, as they did not consider the use of different Hamiltonians by different authors.

[26] Y. Nishida, S. Kida, *Inorg. Chem.* **1988**, *27*, 447–452.

[27] a) E. Escrivà, J. García-Lozano, J. Martínez-Lillo, H. Nuñez, J. Server-Carrió, L. Soto, R. Carrasco, J. Cano, *Inorg. Chem.* **2003**, *42*, 8328–8336 and references cited therein; b) M. Zaręba, K. Drabent, Z. Ciunik, S. Wołowiec, *Inorg. Chem. Commun.* **2004**, *7*, 52–85; c) S. K. Dey, T. S. M. Abedin, L. N. Dawe, S. S. Tandon, J. L. Collins, L. K. Thompson, A. V. Postnikov, M. S. Alam, P. Müller, *Inorg. Chem.* **2007**, *46*, 7767–7781.

[28] G. M. Sheldrick, *Acta Crystallogr., Sect. A* **2008**, *64*, 112–122.

[29] *STOE & CIE GmbH*, X-RED, Darmstadt, Germany, **2002**.

Received: January 19, 2009
Published Online: July 7, 2009

